

Flow-Induced Crystallization of Collagen: A Potentially Critical Mechanism in Early Tissue Formation Supporting Information

Jeffrey A. Paten[†], Seyed Mohammad Siadat[†], Monica E. Susilo[†], Ebraheim N. Ismail[†], Jayson L. Stoner[†], Jonathan P. Rothstein[‡], and Jeffrey W. Ruberti^{*†}

[†] Department of Bioengineering, Northeastern University, 360 Huntington Avenue, Boston, Massachusetts 02115, United States

[‡] Department of Mechanical and Industrial Engineering, University of Massachusetts Amherst, 160 Governors Drive, Amherst, 8 Massachusetts 01003, United States

* Corresponding Author's Email: j.ruberti@neu.edu

Supplementary Movie Captions

Movie S1. Initial fiber creation. A glass microneedle is shown piercing into the droplet of collagen solution. A collagen fiber is created as the needle pulls out of the solution.

Movie S2. Fiber mobility. The mobility of the necking region is shown to demonstrate that the solid structure of the fiber only exists where the extensional strain of drawing was applied.

Movie S3. Fiber drawing with fluorescent beads. The fluorescent beads motions reveal the central recirculation zone visually apparent, as well as the high extensional flow profile at the periphery.

Movie S4. Fiber repair. A short collagen segment, attached to the glass microneedle, is re-inserted into the collagen droplet. The end of the segment triggers repair and continued fiber assembly.

Supporting Information

Calculating the Evaporation Rate

The evaporation of the droplet was measured by shifting the experimental setup from the microscope stage to a scale (CP225D, Sartorius). 125 μL of collagen solution was pipetted onto the coverslip, the dry nitrogen gas was set to the experimental value of 0.022 psi, and the droplet weight was recorded every minute for 5 min. The weight was converted to volume using a solution density of 1 mg/ μL , and the average evaporation rate was calculated to be 2.71 ± 0.21 $\mu\text{L}/\text{min}$. The weight of the droplet at each time point was once again converted to volume and modeled as a hemisphere pinned to an 8 mm disc (the coverslip) to calculate the corresponding surface area of the droplet. The surface area of the droplet, at the time the fiber was drawn, was used in the subsequent section to determine the droplet surface concentration.

Calculating the Droplet Surface Concentration – Evaporation-driven Convective Diffusion Scaling Approach

The Péclet number was calculated to determine if the collagen molecules were able to diffuse into the bulk during evaporation or if the advection from the water molecules exiting the droplet led to surface enrichment. The Péclet number (P_e), a ratio of advective transport to diffusive transport, was calculated as:

$$P_e = \frac{L_c U}{D}, \quad (\text{Eq. S1})$$

where L_c is the characteristic length, U is the average velocity of the boundary, and D is the collagen diffusion coefficient. The characteristic length was calculated to be 45.8 μm using:

$$L_c = \sqrt{2Dt}, \quad (\text{Eq. S2})$$

where t is the time over which evaporation occurred. Fletcher measured the diffusion rate to be 7×10^{-12} m^2/s for a 1 mg/mL solution.¹ Although the diffusion rate is known to decrease with increasing concentration,^{2,3} no studies using higher concentrations were found. The boundary velocity was calculated as:

$$U = \frac{E_r}{A}, \quad (\text{Eq. S3})$$

where E_r is the evaporation rate ($\mu\text{l}/\text{min} = \text{mm}^3/\text{min}$) and A is the surface area of the droplet (mm^2). The evaporation rate, when measured on the scale, was found to be relatively constant. The surface area was calculated under the assumption that the droplet remained pinned to the 8 mm coverslip and maintained a spherical shape. The Péclet number was determined to range from 3.04 – 3.13 between 0 – 3 min (fiber drawn at 2.5 min). The calculation suggests that the collagen molecules were retained at the surface during evaporation without substantial diffusion-driven escape into the bulk. If it is assumed that the evaporation occurred evenly across the surface of the droplet, then the calculated average surface concentration is 11.85 mg/mL, using the surface area at 2.5 min and the thickness of the layer as L_c . However, there will be a local gradient which drives the surface concentration to a higher value than this average.

Calculating the Droplet Surface Concentration – Viscosity Approach

The suppliers of the monomeric collagen (Advanced Biomatrix) have provided a calibration curve, Figure S5, relating the collagen concentration of the solution to the viscosity for 0 to 6 mg/mL. The concentration of the droplet, on the surface and at varying depths, was determined by measuring the viscosity and calculating the concentration from the cubic relationship applied to fit Advanced Biomatrix's data. An assumption was made that the viscosity/concentration relationship holds valid for concentrations in excess of 6 mg/mL.

The viscosity of the droplet surface was measured by adding 2.8 μm magnetic microspheres (14305D, Life Technologies) to the droplet solution and observing their motion in the presence of a magnetic field. Using a force balance between the drag force and the magnetic force, the velocity of the microspheres was used to solve for the viscosity of the solution at the location of the microspheres. The drag force was calculated as:

$$\vec{F}_d = -6\pi\eta R\vec{u}, \quad (\text{Eq. S4})$$

where η is the dynamic viscosity ($\text{kg m}^{-1} \text{s}^{-1}$), R is the bead magnetic particle radius (m), and \vec{u} is the velocity of the magnetic microsphere (m s^{-1}). The magnetic force was calculated as:

$$\vec{F}_M = \frac{V\chi_{bead}}{\mu_0} (\vec{B} \cdot \nabla) \vec{B}, \quad (\text{Eq. S5})$$

where V is the volume of the microsphere (m^3), χ is the magnetic susceptibility of the microspheres (dimensionless), μ_0 is the permeability of vacuum ($4\pi \times 10^{-7} \text{ T m A}^{-1}$), and \vec{B} is the applied magnetic field (T). The resultant force balance equation was:

$$\vec{F}_M + \vec{F}_d = m\vec{a}, \quad (\text{Eq. S6})$$

where the acceleration, a , was determined to be zero as a consequence of the microspheres reaching terminal velocity in under 30 ns when in a ~ 100 cp viscosity solution (the viscosity of the bulk solution of the droplet).

A permanent magnet (BY0Y08-N52, K&J Magnetics, Inc.) was used to provide the magnetic field. A gauss meter placed at the corresponding experimental distance, and the magnetic strength, \vec{B} , was measured as $593 \times 10^{-4} \text{ T}$ with a rate of change, $\frac{\partial B_x}{\partial x}$, of 2.9 T/m. The magnetic susceptibility of the microspheres, χ_{bead} , was determined using a superconducting quantum interference device. The susceptibility was calculated as the initial slope of the magnetization curve multiplied by the 1600 kg/m^3 density of the beads (Figure S6), resulting in a value of 0.512 for χ_{bead} .

The microsphere velocity at the surface of the droplet was measured by introducing the magnet at the fiber drawing time and imaging the microsphere motions at 200x magnification. Random, convective fluctuations within the droplet were isolated from the magnetic field induced velocity by including 1.9 μm non-magnetic, fluorescent beads (G0200, Thermo Scientific) in the solution and subtracting their velocity vector from that of the magnetic microspheres. The net velocity of the magnetic microspheres was determined on the surface of the droplet, as well as at a depth of 20, 40, 60, and 1000 μm below the surface to identify the concentration gradient. The microsphere velocity at each location was then used to calculate viscosity as follows:

$$\eta = \frac{V\chi_{bead}}{6\pi R u_x \mu_0} \left(\frac{\partial B_x}{\partial x} \right) B_x. \quad (\text{Eq. S7})$$

Each viscosity value was then inserted into the polynomial equation from Figure S5 to calculate the collagen concentration distribution throughout the droplet (Figure S7). The plot shows that the viscosity – concentration correlation predicts a droplet surface concentration of $13.98 \pm 3.47 \text{ mg/mL}$. These measurements show the inaccuracy in assuming one concentration for the surface layer as thick as the characteristic length found in the evaporation approach. Instead, there is a steep gradient in concentration from the surface of the droplet to approximately 200 μm deep. The decrease in concentration from 13.98 mg/mL at

the surface to 7.91 mg/mL 20 μm below the surface may explain why the region of highly aligned fibrils on the shell of the fiber was only 5 – 10 μm thick.

Estimation of the Maximum Extensional Strain Rate and the Net Strain on the Forming Fiber

The mass flow rate in the filament is given as:

$$\dot{m} = \rho u_{avg} A, \quad (\text{Eq. S8})$$

where the velocity and the cross-sectional area are unknowns. Continuity requires the mass flow rate to be constant at all locations along the filament because the fluid is incompressible. If we assume a shear free boundary condition at the vapor-fluid interface, then the result is plug flow and a constant velocity across the filament, $u \neq f(r)$. The extension rate is defined as:

$$\dot{\epsilon} = \frac{\partial u}{\partial x}. \quad (\text{Eq. S9})$$

Substituting for the velocity from the mass flow rate equation we find an extension rate that is only dependent on the local radius of the fluid filament:

$$\dot{\epsilon} = \frac{\partial u}{\partial x} = \frac{\dot{m}}{\rho \pi} \frac{\partial(R^{-2})}{\partial x} = \frac{-2\dot{m}}{\rho \pi R^3} \frac{\partial R}{\partial x}. \quad (\text{Eq. S10})$$

To find the extensional strain, we can integrate the extension rate along the filament with time:

$$\epsilon = \int \dot{\epsilon} dt = \int \frac{\partial u}{\partial x} dt = \int \frac{du}{u} = \ln\left(\frac{u_2}{u_1}\right) = 2 \ln\left(\frac{R_1}{R_2}\right). \quad (\text{Eq. S11})$$

Thus by measuring the variation of the filament area as a function of position along the filament it is possible to approximate both the extension rate and the extensional strain accumulated along the filament as it is pulled. Using this approach, a maximum extension rate of approximately $\dot{\epsilon} = 0.5 \text{ s}^{-1}$ was calculated at a location roughly 150 μm along the filament with a total accumulated strain of approximately $\epsilon = 8$.

Extensional Strain Rate Magnification at Object Ends

If we have a system of infinitely stiff, high aspect-ratio objects (*e.g.*, rods or fibrils) embedded in a viscous solution to which a global extensional strain is applied, we can determine the effect of the length, L , of the rods and the width of the gap between them, W , on the inter-rod extensional strain rate, $\dot{\epsilon}_{gap}$ (see Figure S8B). We assume that the extensional strain, ϵ_{global} , is applied and distributed uniformly to the ends of the system. If we define the global extensional strain rate as constant, then:

$$\dot{\epsilon}_{global} = \frac{dU_z}{dz} = C, \quad (\text{Eq. S12})$$

where U_z is the velocity of the system in the z direction of strain. We define the velocity of the each rod as the velocity of its center point which is moving at the local fluid velocity U_z . To determine the extensional strain between two rods, we need the difference in the velocities of the juxtaposed ends. Since each rod end moves at the same speed as its center point (infinite tensile stiffness assumption) the speed of the right side of the left rod is:

$$V_r = V_{gap} - \frac{dU_z}{dz} \left(\frac{W}{2} + \frac{L}{2} \right), \quad (\text{Eq. S13})$$

where V_{gap} is the velocity of the system at the center of the gap between rods. Replace the derivative with the global strain rate and we get:

$$V_r = V_{gap} - \dot{\epsilon}_{global} \left(\frac{W+L}{2} \right). \quad (\text{Eq. S14})$$

For the left end of the right rod, we similarly find:

$$V_l = V_{gap} + \dot{\epsilon}_{global} \left(\frac{W+L}{2} \right). \quad (\text{Eq. S15})$$

The extensional strain rate in the gap is the difference between the two velocities divided by the gap width:

$$\dot{\varepsilon}_{gap} = \frac{(V_l - V_r)}{W} \quad (Eq. S16)$$

or

$$\dot{\varepsilon}_{gap} = \dot{\varepsilon}_{global} \left(\frac{W+L}{W} \right). \quad (Eq. S17)$$

The ratio of the gap extensional strain to the global extensional strain is:

$$\dot{\varepsilon}_{gap} = \dot{\varepsilon}_{global} \left(\frac{W+L}{W} \right) \quad (Eq. S18)$$

or

$$\frac{\dot{\varepsilon}_{gap}}{\dot{\varepsilon}_{global}} = \left(1 + \frac{L}{W} \right). \quad (Eq. S19)$$

We can see immediately that as fibrils grow in length and approach each other, the extensional strain rate in the gap increases to multiple times the global extensional strain rate. As the gap width decreases, we get a hyperbolic increase in the extensional strain which would cause rapid bridging of small gaps through the FIC of available collagen.

References

- (1) Fletcher, G. C. Dynamic Light Scattering from Collagen Solutions. I. Translational Diffusion Coefficient and Aggregation Effects. *Biopolymers* **1976**, 15, 2201-2217.
- (2) Bueno, E. M.; Ruberti, J. W. Optimizing Collagen Transport through Track-Etched Nanopores. *J Memb Sci* **2008**, 321, 250-263.
- (3) Claire, K.; Pecora, R. Translational and Rotational Dynamics of Collagen in Dilute Solution. *J Phys Chem B* **1997**, 101.
- (4) Kress, H.; Stelzer, E. H.; Holzer, D.; Buss, F.; Griffiths, G.; Rohrbach, A. Filopodia Act as Phagocytic Tentacles and Pull with Discrete Steps and a Load-Dependent Velocity. *Proc Natl Acad Sci USA* **2007**, 104, 11633-11638.

Supplementary Figures

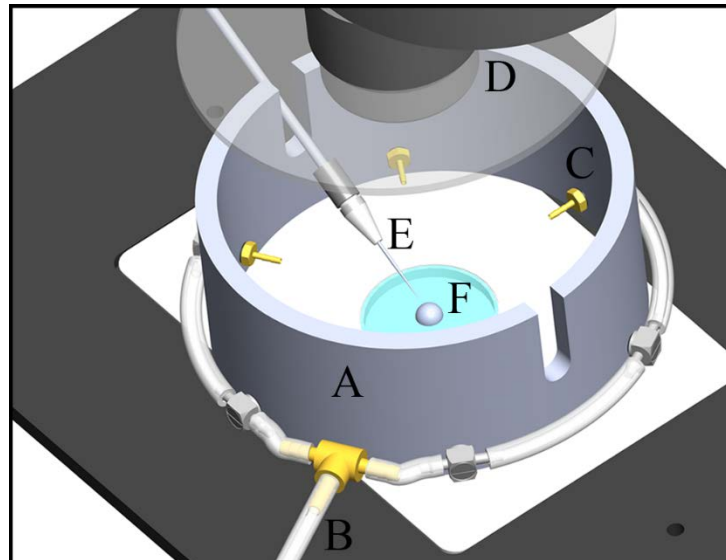


Figure S1. Collagen Fiber Drawing Setup. (A) Nitrogen diffusing chamber to maintain <5% room humidity. (B) Primary inlet of dry nitrogen gas. (C) One of six gas diffusers. (D) Chamber lid, attached to the condenser lens of an inverted microscope to maintain optical access. (E) Glass microneedle on a robotic arm for drawing the fiber. (F) Droplet of collagen solution on an 8 mm coverslip for repeatable geometric constraint.

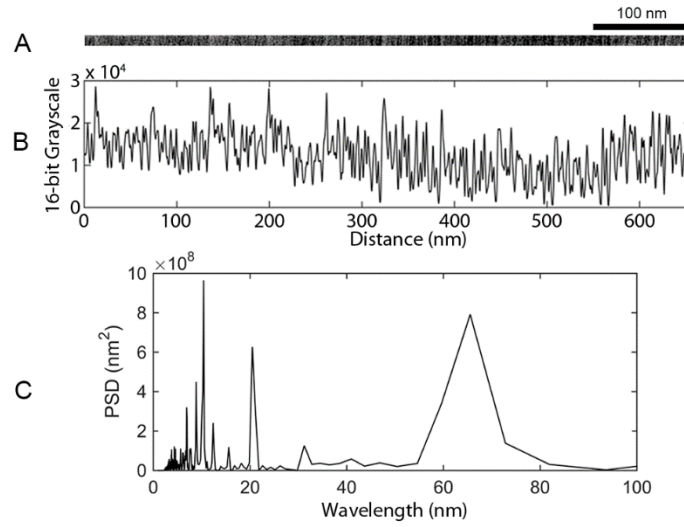


Figure S2. (A) The cropped region of a banded fibril. (B) A plot of each column's average grayscale value. (C) The Power Spectral Density plot used to determine the banding periodicity.

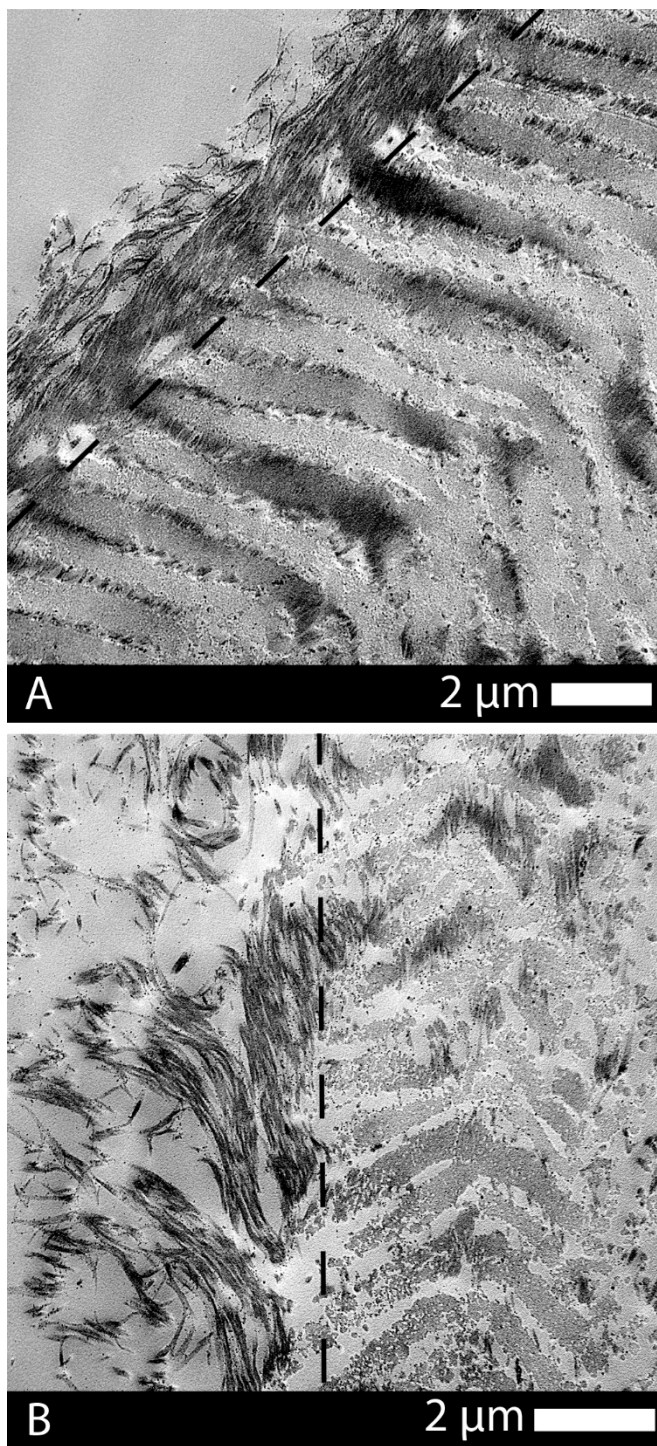


Figure S3. (A) Telo-fiber incubated for 1 hour in a loaded configuration. (B) Telo-fiber incubated for 48 hours in an unloaded configuration. The dashed line in (A) and (B) denotes the boundary between the fiber shell and the transition to core structure.

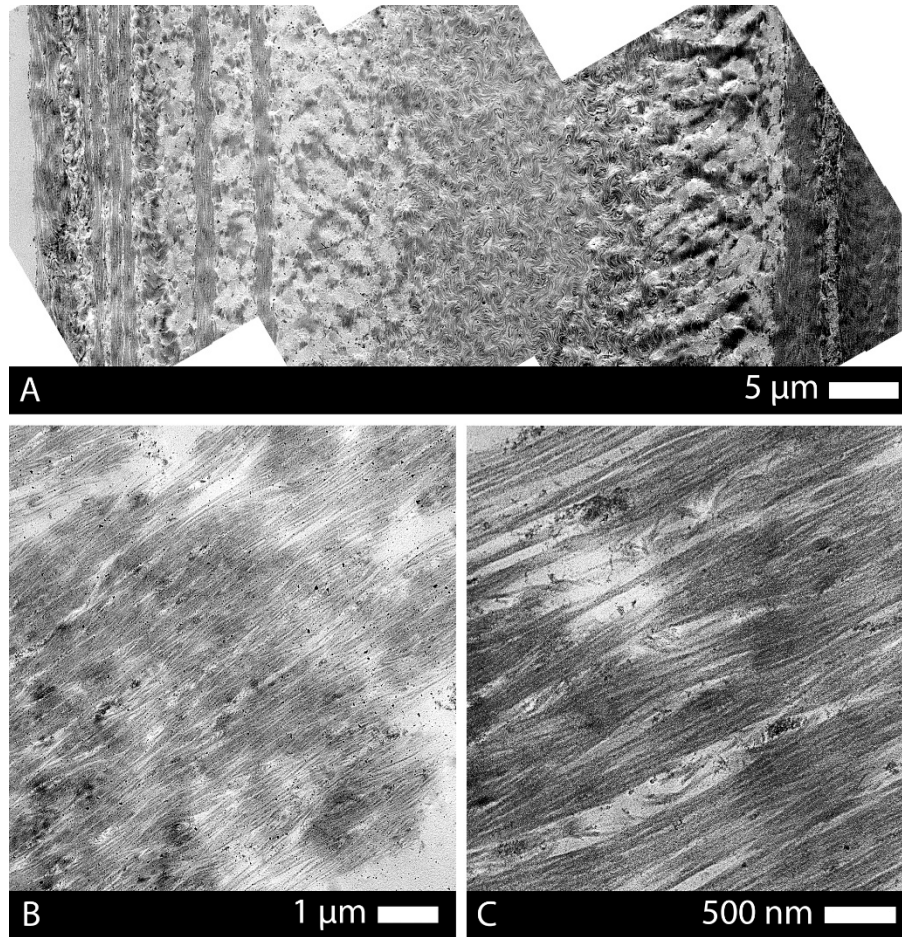


Figure S4. TEM thin sections of drawn telo-fibers. (A) The fiber morphology transitions from densely packed fibrils on the periphery to sparse, isotropic fibrils at the core. Repeating bands of aligned fibrils indicate that the shell of the fiber passes in and out of the TEM section. (B,C) The fiber shell is shown at increasing magnification. The fibrils have a clear, uniaxial alignment yet lack control over the interfibrillar spacing.

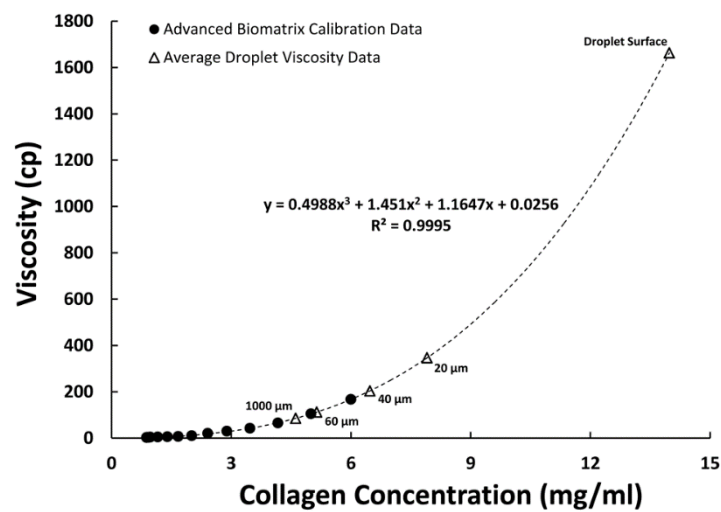


Figure S5. The relationship between collagen solution concentration and viscosity. The calibration curve was generated using data provided by Advanced Biomatrix (filled black circles). The average viscosity measurements (unfilled black triangles) made on the droplet and at depths below the surface (data point labels) have been plotted along the extrapolated curve, generated from Advanced Biomatrix's data.

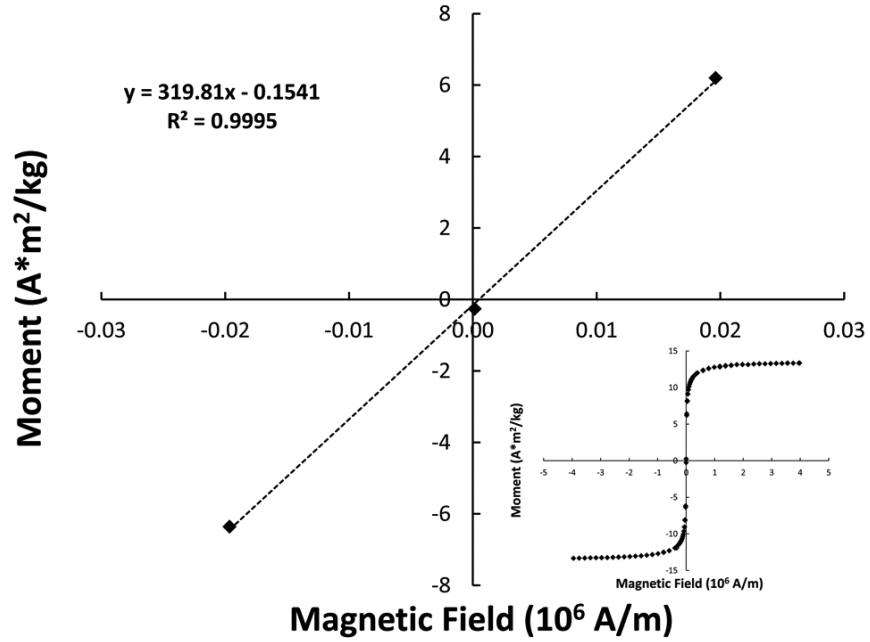


Figure S6. The magnetic response of the microspheres across a range of magnetic field strengths. The slope of the initial response, $319.81 \times 10^{-6} \text{ m}^3/\text{kg}$, is used to calculate the susceptibility parameter. The inset shows the response of the microspheres across the entire $\pm 5 \text{ T}$ range.

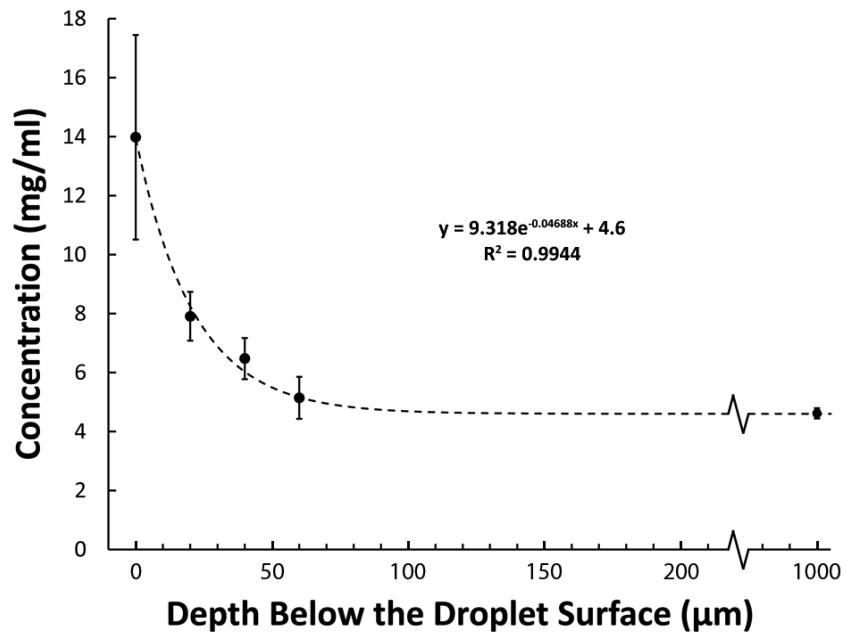


Figure S7. The gradient of collagen concentration throughout the droplet. Viscosity measurements were taken from the droplet at different depths and converted into concentration values using the curve fit equation from Figure S5.

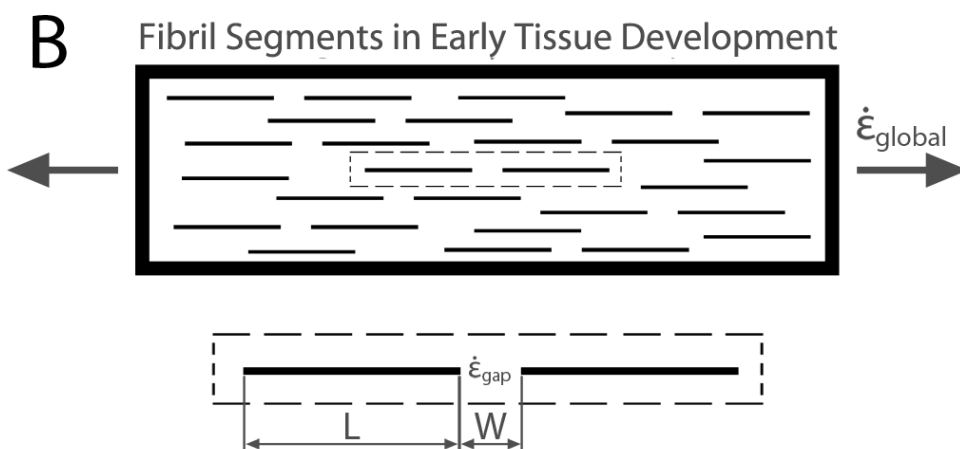
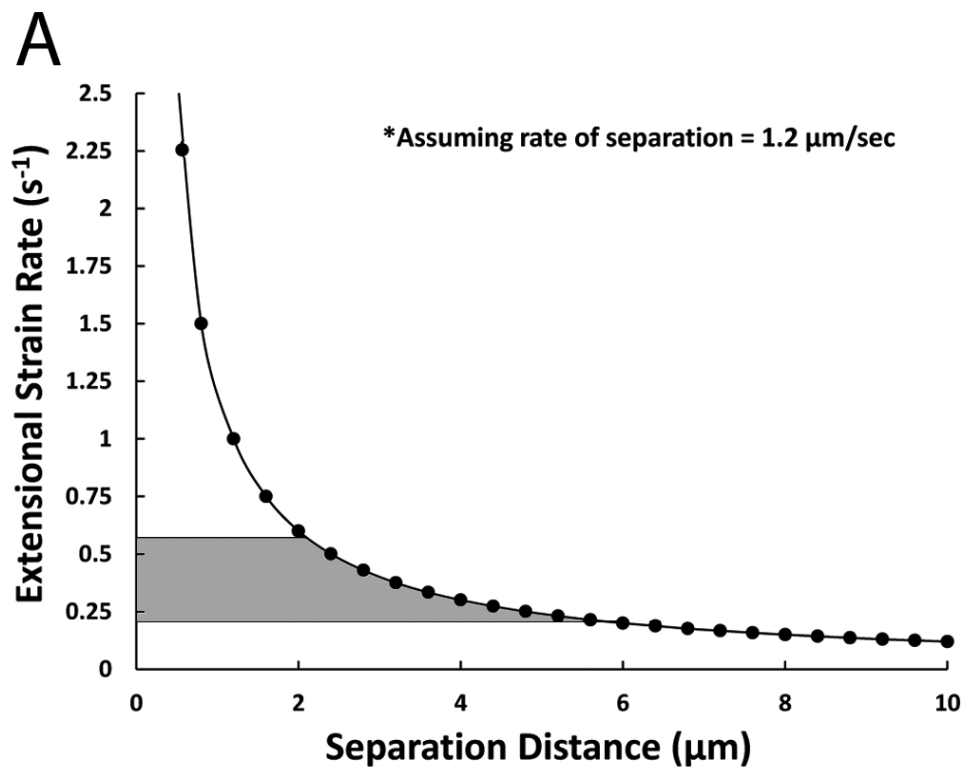


Figure S8. (A) The extensional strain rate generated by the retraction of two objects (*e.g.*, cell filopodia), as a function of separation distance. The velocity was chosen in reference to the maximum velocities observed by Kress *et al.*⁴. The highlighted gray region shows the overlap with the extensional strain rates ($0.39 \pm 0.18 \text{ s}^{-1}$ (avg \pm std.dev)) observed in the fiber pulling experiments. The data suggests that initial fibrillogenesis may generate fibrils that are approximately 5 – 10 μm in length. (B) Once multiple fibrils are present, a global extensional strain applied to the fibrils causes stress extensional strain amplification in the gaps between the fibrils. The inset image shown below depicts two aligned fibril segments, with length, L , and a gap distance of W . The resulting gap extensional strain rate is equal to the global extensional strain, scaled up by $1 + L/W$ (see Eq. S19). In the presence of soluble monomer, global extensional strains at sub-threshold rates can still trigger FIC preferentially in the gap regions, and lead to the fusion of fibril segments.